Computer Modelling in Ocean Engineering 91, Arcilla et al. (eds) © 1991 Balkema, Rotterdam. ISBN 90 5410 024 9

# Modulation of water waves through an uneven sea floor

Ching-Yun Yueh, C.R.Chou & W.K.Weng
*National Taiwan Ocean University, Department of River & Harbour Engineering, Taiwan*

ABSTRACT: Transformations of finite amplitude progressive waves due to an uneven sea floor were studied both numerically as well as experimentally. The numerical analyses were carried out in two steps. Linear wave theory was used as a first order approximation. Solutions thus obtained were then used as initial conditions for the nonlinear wave analysis. As a verification of the numerical results, experiments were then carried out in the laboratory of the Department of River and Harbour Engineering of the National Taiwan Ocean University. The agreements are satisfactory. This paper summarizes the present results.

## 1 INTRODUCTION

Transformation of finite amplitude waves passing an obstacle or an uneven sea floor has been studied previously by many researchers. However, one of the main difficulties encountered in the numerical analyses is that, the boundaries and/or domains are sometimes not continuous. In this paper, a numerical method proposed by Chou et al. (Chou et al., 1988) was adopted to overcome this difficulty. Analyses have shown that, the boundary element method used could not only handle problems of complex terrains more efficiently, but also reduce the computation time and memory storage.

Three kinds of sea floor topography were used for the numerical modeling. These are: a submerged dike of trapezoid shape, a gentle sloping beach, and a steep bank. It were found that, as wave shoals, its wave length shortens and its amplitude accumulates as compared with its values for the deep water case. These results are in satisfactory agreement with experimental results available. It seems that the numerical procedure proposed in this paper provides an efficient method in calculating wave transformation problems of similar category.

## 2 SMALL AMPLITUDE WAVE THEORY

Consider a region of water having finite depth, h, and bounded below by an impermeable sea floor. Cartesian coordinates, (x,z), are applied, where the z-axis is directed positively upward, and z = 0 is the undisturbed free surface. For simplicity, the region was further divided into three sub-regions, I, II, and III. Both sub-regions I and III have constant water depth, whereas in sub-region II the water depth is arbitrary. Sub-regions I and III are assumed to be beyond the disturbances caused by the sea floor topography. As shown in Fig. 1a, the origin of the coordinates is located in sub-region II, where the left side is unbounded. In Fig. 1b, on the other hand, the left side boundary coincides with the origin. The usual assumptions of water being inviscid, incompressible and wave motion irrotational have being adopted here in the analysis. Waves arriving from the right hand side of these figures are of small amplitude type, having a constant frequency $\sigma$ and amplitude $\zeta_0$.

Due to the assumptions made earlier, fluid motions of all sub-regions will, therefore, have velocity potentials which satisfy the Laplace equation. These velocity potentials can be expressed as: $\Phi(x,z;t) = g\zeta_0/\sigma \cdot \phi(x,z) \cdot \exp(i\sigma t)$

### 2.1 Velocity potentials in domain I and III

Consider Fig. 1a where the two imaginary boundaries are assumed to be located far away from the origin. Since sub-regions I and III are assumed to be beyond influences of the sea floor topography, one has $\varphi_I(x,z)$ for the sub-region I:

$$\varphi_1(x,z)= \quad (2.1)$$
$$\left[e^{ik(x-\ell_1)}+\phi_1 e^{-ik(x-\ell_1)}\right]\frac{\cosh k(h+z)}{\cosh kh}$$

where $\ell_1$ is the horizontal distance between the imaginary boundary I and the origin o of the coordinate, k is the root of $\sigma^2 h/g = kh \tanh(kh)$. The first term in parenthesis on the right side of Eq. (2.1) is the potential function of the incident wave, and the second term is that of the reflected, both in complex forms.

On the imaginary boundary, where $x = \ell_1$, the potential function and its normal derivative in the positive x-direction are given by:

$$\varphi_1(\ell_1,z)=(1+\phi_1)\frac{\cosh k(h+z)}{\cosh kh} \quad (2.2)$$

$$\overline{\varphi}_1(\ell_1,z)=ik(1-\phi_1)\frac{\cosh k(h+z)}{\cosh kh} \quad (2.3)$$

Similarly, the potential function on the imaginary boundary of the transmitted region, i.e., in the third region, $x = -\ell_2$, together with its normal derivative in the negative x-direction can be expressed as:

$$\varphi_3(x,z)=\phi_2 e^{ik(x+\ell_2)}\frac{\cosh k'(qh+z)}{\cosh k'qh} \quad (2.4)$$

$$\varphi_3(-\ell_2,z)=\phi_2\frac{\cosh k'(qh+z)}{\cosh k'qh} \quad (2.5)$$

$$\overline{\varphi}_3(-\ell_2,z)=-ik\phi_2\frac{\cosh k'(qh+z)}{\cosh k'qh} \quad (2.6)$$

where K' is the root of $\sigma^2 qh/g = k'qh \tanh(k'qh)$. As for the case shown in Fig. 1b, due to the assumption of an impermeable boundary on one side, the transmitted term is identically zero.

## 2.2 The governing equation and the boundary conditions in sub-region II

i) Under the assumptions made, the governing equation for small amplitude waves is expressed as:

$$\frac{\partial^2\phi}{\partial x^2}+\frac{\partial^2\phi}{\partial z^2}=0 \quad (2.7)$$

ii) The free surface boundary condition. A combination of the kinematic, dynamic boundary conditions together with the requirement of constant pressure yields:

$$\overline{\phi}=\sigma^2/g\cdot\phi \quad (2.8)$$

iii) Velocity normal to the impermeable sea floor should be zero:

$$\partial\phi/\partial\nu=0 \quad (2.9)$$

iv) For the case shown in Fig. 1b, the velocity normal to the impermeable boundary is also zero:

$$\partial\phi/\partial\nu=0 \quad (2.10)$$

## 2.3 Dynamic boundary conditions on the imaginary boundaries and the coefficients of reflection and transmission

In sub-regions I, II, and III of Fig. 1a, the requirements of continuity of mass- and energy fluxes yield:

$$\phi(\ell_1,z)=\varphi_1(\ell_1,z) \quad (2.11)$$

$$\overline{\phi}(\ell_1,z)=\overline{\varphi}_1(\ell_1,z) \quad (2.12)$$

$$\phi(-\ell_2,z)=\varphi_3(-\ell_2,z) \quad (2.13)$$

$$\overline{\phi}(-\ell_2,z)=\overline{\varphi}_3(-\ell_2,z) \quad (2.14)$$

Substituting Eq. (2.2) into Eq. (2.11), multiplying cosh k(h+z), and integrating from z = -h to z = 0, one then has the reflection coefficient, $\phi_1$, in terms of the potential function $\phi_1$, as:

$$\phi_1=\frac{k}{N_0\sinh kh}\int_{-h}^{0}\phi\cosh k(h+z)\,dz \quad (2.15)$$

where

$$N_0=\tfrac{1}{2}(1+2kh/\sinh kh)$$

The coefficient of transmission is acquired by substituting Eq. (2.5) into Eq. (2.13), multiplying with cosh k'(qh+z), and integrating from z = -qh to 0. It has the following form:

$$\phi_2=\frac{k'}{N_0'\sinh k'qh}\int_{-qh}^{0}\phi\cosh k'(qh+z)\,dz \quad (2.16)$$

where

$$N_0'=\tfrac{1}{2}(1+2k'qh/\sinh k'qh)$$

## 2.4 The Green's function

According to Green's second identity law, the velocity potential of any arbitrary point (x,z) inside domain II can be determined by the velocity potential on the boundary together with its first normal derivative, that is:

$$\phi(x,z)$$

$$=\frac{1}{2\pi}\int_\Gamma\left[\frac{\partial\phi(\xi,\eta)}{\partial\nu}\ln\frac{1}{r}-\phi(\xi,\eta)\frac{\partial}{\partial\nu}\left(\ln\frac{1}{r}\right)\right]ds \quad (2.17)$$

where $\phi(\xi,\eta)$ is the potential function on the boundary of domain II, $\partial\phi(\xi,\eta)/\partial\nu$ is the first normal derivative, and $\ln(1/r)$ is the solution of Laplace equation. r is the distance between any interior point within domain II and a point located on the boundary. The velocity potential for any boundary point, $(\xi',\eta')$ , is then expressed as:

$$\phi(\xi',\eta') = \frac{1}{\pi}\int_{\Gamma}\left[\frac{\partial\phi(\xi,\eta)}{\partial\nu}\ln\frac{1}{r}-\phi(\xi,\eta)\frac{\partial}{\partial\nu}\left(\ln\frac{1}{r}\right)\right]ds \tag{2.18}$$

## 2.5 Discretization of the integral equation

Dividing the curves enclosing the sub-region II into N small segments counterclockwise, then the physical quantities in each segment can be treated as to have lnear variations. It follows that, Eq. (2.18) can be written in the following form:

$$\phi_i(\xi,\eta) + \frac{1}{\pi}\sum_{j=1}^{N}\int_{\Gamma_j}\left(\phi_j(\xi,\eta)\cdot M_1+\phi_{j+1}(\xi,\eta)\cdot M_2\right)\frac{\partial}{\partial\nu}\ln\frac{1}{r}ds = \frac{1}{\pi}\sum_{j=1}^{N}\int_{\Gamma_j}\left(\overline{\phi}_j(\xi,\eta)\cdot M_1+\overline{\phi}_{j+1}(\xi,\eta)\cdot M_2\right)\ln\frac{1}{r}d\varepsilon \tag{2.19}$$

where $M_1$ and $M_2$ are weighting functions. Eq. (2.19) can be expressed in a matrix form:

$$[\phi] = [0][\overline{\phi}] \tag{2.20}$$

Dividing the curve enclosing the sub-region II further into: the first imaginary boundary, the free surface, the second imaginary boundary (for the case shown in Fig. 1b, this equals to the impermeable boundary), and the sea floor, and with their velocity potentials and normal derivatives expressed as: $\phi_1$ , $\overline{\phi}_1$ , $\phi_2$ , $\overline{\phi}_2$ , $\phi_3$ , $\overline{\phi}_3$ , $\phi_4$ , $\overline{\phi}_4$ , respectively, one has:

$$\begin{bmatrix}\phi_1\\ \phi_2\\ \phi_3\\ \phi_4\end{bmatrix} = \begin{bmatrix}O_{11} & O_{12} & O_{13} & O_{14}\\ O_{21} & O_{22} & O_{23} & O_{24}\\ O_{31} & O_{32} & O_{33} & O_{34}\\ O_{41} & O_{42} & O_{43} & O_{44}\end{bmatrix}\begin{Bmatrix}\overline{\phi}_1\\ \overline{\phi}_2\\ \overline{\phi}_3\\ \overline{\phi}_4\end{Bmatrix} \tag{2.21}$$

where the number of segments of these boundaries are $N_1$, $N_2$, $N_3$ and $N_4$, respectively.

## 2.6 The velocity potential for small amplitude waves

For the case shown in Fig. 1a, substituting of Eq. (2.15) into Eq. (2.3), and from Eq. (2.12) one has the normal derivatives of the velocity potential for each nodes on the boundary $x = \ell_1$ , given by:

$$\phi_1(P) = 2ik\frac{\cosh k(h+z_p)}{\cosh kh} + \sum_{r=1}^{N1}\overline{\phi}_1(r)f_1(r,p)\cdot\Delta z_p \tag{2.22}$$

where

$$f_1(r,p) = \frac{ik^2\cosh k(h+Zr)\cosh k(h+Zp)}{N_0\sinh kh\cosh kh}$$

Similarly, substituting Eq. (2.16) into Eq. (2.6) and from Eq. (2.14), one has the normal derivatives of the velocity potential for each nodes on the boundary $x = -\ell_2$:

$$\overline{\phi}_3(q) = \sum_{r=1}^{N3} f_2(r,q)\phi_3(r)\cdot\Delta z_s \tag{2.23}$$

where

$$f_2(r,q) = \frac{ik'^2\cosh k'(qh+Zr)\cosh k'(qh+Zq)}{N_0'\sinh K'qh\cosh k'qh}$$

Writing Eqs. (2.22) and (2.23) in matrix forms:

$$\{\overline{\phi}_1\} = \{z'\} + \{F'\}\{\phi_1\} \tag{2.24}$$

$$\{z\} = 2ik\frac{\cosh k(z_p+h)}{\cosh kh}$$

$$\{F'\} = f_1(i,j)\cdot\Delta z_j \qquad (i;j=1\sim N_1)$$

$$\{\overline{\phi}_3\} = \{R'\}\{\phi_3\} \tag{2.25}$$

$$\{R'\} = f_2(i,j)\cdot\Delta z_j \qquad (i;j=1\sim N_3)$$

After substituting Eqs. (2.8), (2.9), (2.24) and (2.25) into Eq. (2.21) and rearranging, one has then a linear system of equations for the velocity potentials of small amplitude waves on the boundaries of sub-region II in Fig. 1a:

$$\begin{bmatrix}O_{11}F'-I & O_{12}\sigma^2/g & O_{13}R' & 0\\ O_{21}F' & O_{22}\sigma^2/g-I & O_{23}R' & 0\\ O_{31}F' & O_{32}\sigma^2/g & O_{33}R'-I & 0\\ O_{41}F' & O_{42}\sigma^2/g & O_{43}R' & -I\end{bmatrix}\begin{Bmatrix}\phi_1\\ \phi_2\\ \phi_3\\ \phi_4\end{Bmatrix} = -\begin{bmatrix}O_{11}\\ O_{21}\\ O_{31}\\ O_{41}\end{bmatrix}\cdot[Z'] \tag{2.26}$$

Which can be expressed more compactly as:

$$\begin{Bmatrix}\phi_1\\ \phi_2\\ \phi_3\\ \phi_4\end{Bmatrix} = -[B]^{-1}\begin{bmatrix}O_{11}\\ O_{21}\\ O_{31}\\ O_{41}\end{bmatrix}[Z'] \qquad (2.27)$$

$$[B] = \begin{bmatrix} O_{11}F'-I & O_{12}\sigma^2/g & O_{13}R' & 0\\ O_{21}F' & O_{22}\sigma^2/g-I & O_{23}R' & 0\\ O_{31}F' & O_{32}\sigma^2/g & O_{33}R'-I & 0\\ O_{41}F' & O_{42}\sigma^2/g & O_{43}R' & -I \end{bmatrix}$$

Eq. (2.27) can be used to calculate the velocity potentials of the nodes on the boundary. The free surface elevation on these nodes can be calculated from:

$$\zeta = -\frac{1}{g}\frac{\partial\Phi_2}{\partial t} = -i\phi_2\cdot\zeta_0\cdot e^{i\sigma t} \qquad (2.28)$$

For an incident wave with prescribed amplitude, $\zeta_0$, phase, $\sigma t$, the surface elevations on each node can thus be calculated accordingly.

For the case of standing waves shown in Fig. 1b, there are only two sub-regions, enclosed by an impermeable left side, velocity potentials on the boundardies of Fig. 1b can be acquired, by substituting Eqs. (2.8), (2.9), (2.10) and (2.24) into Eq. (2.21):

$$\begin{bmatrix} O_{11}F'-I & O_{12}\sigma^2/g & 0 & 0\\ O_{21}F' & O_{22}\sigma^2/g-I & 0 & 0\\ O_{31}F' & O_{32}\sigma^2/g & -I & 0\\ O_{41}F' & O_{42}\sigma^2/g & 0 & -I \end{bmatrix}\begin{Bmatrix}\phi_1\\ \phi_2\\ \phi_3\\ \phi_4\end{Bmatrix} = -\begin{bmatrix}O_{11}\\ O_{21}\\ O_{31}\\ O_{41}\end{bmatrix}[Z'] \qquad (2.29)$$

where free surface elevations can be calculated using Eq. (2.28).

## 3 FINITE AMPLITUDE WAVES

Transformation of nonlinear waves was studied using linear solutions derived earlier as initial conditions. Together with the full free surface conditions, they were substituted into Green's integral equation. It is rather difficult to obtain analytic solutions for the reflection, as well as transmission, coefficients of finite amplitude waves. This difficulty was avoided by using the Sommerfeld radiation condition on the imaginary boundary of subregion II.

### 3.1 Boundary conditions

i) The dynamic and kinematic boundary conditions on the free surface are:

$$\frac{\partial\Phi}{\partial t} + \frac{1}{2}\left[\left(\frac{\partial\Phi}{\partial x}\right)^2 + \left(\frac{\partial\Phi}{\partial z}\right)^2\right] + g\zeta = 0 \qquad (3.1)$$

$$\frac{\partial\zeta}{\partial t} = \frac{\partial\Phi}{\partial z} - \frac{\partial\Phi}{\partial x}\cdot\frac{\partial\zeta}{\partial x} \qquad (3.2)$$

ii) Radiation condition on the imaginary boundary

To calculate surface elevations due to finite amplutide waves, the Sommerfeld radiation condition is applied for the imaginary boundaries in this study:

$$\frac{\partial\Phi}{\partial x} = -\frac{k}{\sigma}\cdot\frac{\partial\Phi}{\partial t}, \quad x=l_1 \qquad (3.3)$$

$$\frac{\partial\Phi}{\partial x} = \frac{k}{\sigma}\cdot\frac{\partial\Phi}{\partial t}, \quad x=-l_2 \qquad (3.4)$$

For the case shown in Fig. 1b, only Eq. (3.3) is applied.

iii) At the impermeable sea floor:

$$\partial\Phi / \partial\nu = 0 \qquad (3.5)$$

iv) For standing waves in Fig. 1b, on the impermeable bank:

$$\partial\Phi / \partial\nu = 0 \qquad (3.6)$$

### 3.2 Finite differentiation

i) The free surface boundary conditions

Expressing $\partial\Phi/\partial x, \partial\Phi/\partial z$ of the free surface boundary conditions in terms of components normal and tangential to water surface:

$$\frac{\partial\Phi}{\partial x} = \frac{\partial\Phi}{\partial n}\sin\beta - \frac{\partial\Phi}{\partial s}\cos\beta \qquad (3.7)$$

$$\frac{\partial\Phi}{\partial z} = \frac{\partial\Phi}{\partial n}\cos\beta + \frac{\partial\Phi}{\partial s}\sin\beta \qquad (3.8)$$

where $\beta$ is the angle between adjacent nodal points of the free surface and the horizontal axis. Substitution of Eqs. (3.7) and (3.8) into Eq. (3.2) and rearranging, one has the nonlinear free surface elevation in a finite difference form:

$$\zeta_j^{k+1} = \zeta_j^{k} + \frac{\Delta t}{2}\left[\frac{1}{\cos\beta}(\Phi_j^{-k+1}) + \frac{1}{\cos\beta}(\Phi_j^{-k})\right] \qquad (3.9)$$

The nonlinear velocity potential and its normal derivative on the surface are related by:

$$(\Phi_j^{-k+1}) = \frac{1-c}{b}\Phi_j^{k+1} + \frac{c}{b}\Phi_{j-1}^{k+1} - \frac{s}{b} \qquad (3.10)$$

where a, b, and c are given as:

$$a = \Phi_j^k - g\cdot\Delta t\cdot \zeta_j^k - 1/2\cdot g\cdot(\Delta t)^2\,\frac{(\overline{\Phi}_j^k)}{\cos\beta} \tag{3.11}$$

$$b = -\frac{g(\Delta t)^2}{2\cos\beta} - \frac{\Delta t}{2}(\overline{\Phi}_j^k) \tag{3.12}$$

$$c = -\frac{\Delta t[\Phi_j^k - \Phi_{j-1}^k]}{2(\Delta s)^2} \tag{3.13}$$

ii) The radiation conditions

The radiation conditions can be discritized into:

$$(\overline{\Phi}_j^{k+1})_I = [-(\Phi_j^{k+1})_I + (d_j)_I]/e \tag{3.14}$$

$$(\overline{\Phi}_j^{k+1})_{II} = [-(\Phi_j^{k+1})_{II} + (d_j)_{II}]/e' \tag{3.15}$$

with d and e known constants:

$$(d_j)_I = (\Phi_j^k)_I + (\overline{\Phi}_j^k)_I\cdot\left(\frac{\sigma\Delta t}{-2k}\right)$$
$$(d_j)_{II} = (\Phi_j^k)_{II} + (\overline{\Phi}_j^k)_{II}\cdot\left(\frac{\sigma\Delta t}{-2k'}\right) \tag{3.16}$$

$$e = \frac{\sigma\Delta t}{2k}$$
$$e' = \frac{\sigma\Delta t}{2k'} \tag{3.17}$$

In the equations given above, the subscripts I and II denote the imaginary boundaries I and II, respectively. For the case of Fig. 1b only Eq. (3.16) is used.

### 3.3 Solution of the velocity potential for finite amplitude waves

In a way similar to those described in Sec. 2.4 and Sec. 2.5, by substituting Eqs. (3.5), (3.10), (3.14) and (3.15) into Eq. (2.21), one will have a linear system of equations for the velocity potentials of finite amplitude waves on the boundaries:

$$\begin{bmatrix} -O_{11}/e-I & O_{12}[(\frac{1-c}{b})_j+(\frac{c}{b})_{j+1}] & -O_{13}/e' & 0 \\ -O_{21}/e & O_{22}[(\frac{1-c}{b})_j+(\frac{c}{b})_{j+1}]-I & -O_{23}/e' & 0 \\ -O_{31}/e & O_{32}[(\frac{1-c}{b})_j+(\frac{c}{b})_{j+1}] & -O_{33}/e'-I & 0 \\ -O_{41}/e & O_{42}[(\frac{1-c}{b})_j+(\frac{c}{b})_{j+1}] & -O_{43}/e' & -I \end{bmatrix} \begin{Bmatrix} \Phi_1 \\ \Phi_2 \\ \Phi_3 \\ \Phi_4 \end{Bmatrix}$$
$$= \begin{bmatrix} O_{11} & O_{12} & O_{13} \\ O_{21} & O_{22} & O_{23} \\ O_{31} & O_{32} & O_{33} \\ O_{41} & O_{42} & O_{43} \end{bmatrix} \begin{bmatrix} -d_I/e \\ a/b \\ -d_{II}/e' \end{bmatrix} \tag{3.18}$$

Solution of this equation leads one to the nonlinear velocity potentials and their derivatives on the nodal points. Free surface elevations can be calculated from Eq. (3.9).

For the case shown in Fig. 1b, one may substitute Eqs. (3.5), (3.6), (3.10) and (3.14) into Eq. (2.21) to get a linear system of equations for the velocity potentials on the boundary:

$$\begin{bmatrix} -O_{11}/e-I & O_{12}[(\frac{1-c}{b})_j+(\frac{c}{b})_{j+1}] & 0 & 0 \\ -O_{21}/e & O_{22}[(\frac{1-c}{b})_j+(\frac{c}{b})_{j+1}]-I & 0 & 0 \\ -O_{31}/e & O_{32}[(\frac{1-c}{b})_j+(\frac{c}{b})_{j+1}] & -I & 0 \\ -O_{41}/e & O_{42}[(\frac{1-c}{b})_j+(\frac{c}{b})_{j+1}] & 0 & -I \end{bmatrix} \begin{Bmatrix} \Phi_1 \\ \Phi_2 \\ \Phi_3 \\ \Phi_4 \end{Bmatrix}$$
$$= \begin{bmatrix} O_{11} & O_{12} \\ O_{21} & O_{22} \\ O_{31} & O_{32} \\ O_{41} & O_{42} \end{bmatrix} \begin{bmatrix} -d_I/e \\ a/b \end{bmatrix} \tag{3.19}$$

Eq. (3.19) is be used to calculate the nonlinear velocity potentials on the nodal points. Normal derivatives of the velocity potentials and free surface elevations can be calculated using Eqs. (3.10), (3.14), (3.15) and (3.9).

## 4 THE NUMERICAL ANALYSES

Figures 2a, 2b, and 2c show the cases studied in this paper. Optimal computational effort could be achieved, when the elements of the free surface and sea floor both have the same discretization length. For numerical stability, this length must be smaller than 0.2h, with h the water depth in the sub-region I.

The dimensionless period of the incident waves was chosen to be $\sigma^2 h/g = 0.25 \sim 1.0$. Wave heights were set uniformly equal to $\zeta_0/h = 0.05$. In the Figures shown below, surface elevations are calculated from finite amplitude waves. They were plotted in a time interval of T/8 to demonstrate the changes within a half-period.

### 4.1 Gradually varying sea floor

Fig. 2a shows, schematically, a gradually changing sea bottom. This was used to demonstrate the influences of sea floor on wave evolution. Water depth in the sub-region III was assumed equal to qh = 0.25h. Four bed slopes, S = 0, 5h, 10h, and 20h, were studied. Numbers of discretization for the free surface and sea floor were varied accordingly, for stability reasons mentioned before. Table 1 lists the number of segments used for each case. Changes of water surface elevations, as the waaves, with $\sigma^2 h/g = 0.25$, 0.5 and 1.0, passing over various sea floors conditions are shown in Figs. 4, 5, and 6, respectively.

These figures demonstrated that, as waves shoaled, wave heights increases with decreasing wave lengths. Wave set-ups in shallow water region are also clearly evident in these figures.

### 4.2 The case of a submerged trapezoidal dike

For the case of finite amplitude waves passing a submerged trapezoidal dike, Fig. 2b shows a definition sketch. The two imaginary boundaries are both located at distances 10 (ten) times the water depth away from the base of the dike. In all calculations presented here, the dike was located at a depth qh = 0.25h below water surface. The width is B = 2h. For rectangular shaped dike, changes of surface elevations are shown in Figs. 7a, 7b, 7c, and 7d for dimensionless periods $\sigma^2 h/g = 0.25$, 0.5, 0.75 and 1.0, respectively. Figs. 8a, 8b, 8c and 8d are for the case of trapezoidal dike. The length of the slope was 10h. Dimensionless periods are the same as before. From these results, it is evident that, rectangular shaped dikes affect the evolution processes more profoundly than trapezoidal dikes. Partially standing waves are seen to form on the dike, and waves that passed through the dike are smaller, as compared with the case of trapezoidal dikes.

### 4.3 The steep-bank

Figs. 9a, 9b, and 9c show results of waves approaching a steep bank for dimensionless periods $\sigma^2 h/g = 0.25$, 0.5, and 0.75, respectively. The shallow water region has a depth of qh = 0.25h, and the horizontal length of the sloping beach is s = 10h. These figures show that water levels were aroused, which are characteristic for finite amplitude waves.

## 5 THE EXPERIMENTS

The experiments were conducted in a wave flume, located in the Harbor Engineering Laboratory of the Department of River and Harbor Engineering, National Taiwan Ocean University. The wave flume is 50 m long, 1.8 m wide. Piston type wave generator was used to generate incident waves. Surface elevations was measured by capacitance wave gauge. A wave recorder was also used to record the wave forms simultaneously.

For the case shown in Fig. 2a, water depths in the shallow water region were kept equal to q = 0.1 and 0.2. The height of the "sea floor" in this region was fixed to equal to 36 cm during the experiment, for experimental convenience. Water was then filled into the wave flume until a depth of 40 cm (q = 0.1) or 45 cm (q = 0.2) has been reached. The slopes of the beach were varied from s = 0, 2, to 4. Fig. 3 shows these experimental configureations schematically. Three nondimensional periods, $\sigma^2 h/g = 0.3$ and 0.5, were chosen for incident waves. Wave heights were selected using the criteria that: they will not break when reaching the region of variable depth or in the constant-depth shallow water re-tion.

Initially, the wave gauge was installed 1 m away from the intersection point of the slope and the sallow water region. It is believed that, here in this location, disturbances caused by wave shoalling are relatively small. After the passage of approximately two or three waves, recording was initiated, while, simultaneously, wave gauge was shifted slowly in the direction of wave propagation. The travel speed of the wave gauge was kept much smaller than the wave celerity. In this way, the maxima and minima of the surface fluctuations in the shallow water region could be detected. As a result, the envelope of these progressive waves in this region was determined. In all the experiments conducted, the distance of the wave gauge movement was 6 m, approximately.

Since the movement of wave gauge was kept slow, to avoid possible interferences caused by reflected waves, the experiments were conducted stepwise. Waves were generated

only for approximately 1 ~ 1.5 minutes. After the passage of these waves, wave gauge was stalled, to be restarted for the next experiment from here. Wave envelope was then synthesized from several measuring steps.

### 5.1 Comparisons and discussions

The experimental results are shown in Figs. 10b ~ 21b. Shown in these figures, are the relations between wave envelope and the coordinates of x-axis in shallow water region. Straight line connecting the points indicated by o is the still water level (SWL). Curves connecting the peaks below the SWL are the envelopes for the crests, whereas those connecting peaks above the SWL are the trough envelopes. As is clear from these figures, vertical distances between SWL and crest envelopes are larger than those between SWL and trough envelopes. These are indications that, after passing through the variable depth region, these incoming waves tend to raise the mean water level. These were also demonstrated by the numerical calculations. Another interesting fact is that, envelopes in these figures show little variations, which indicates that, when waves arriving in the shallow water area, there is not much changes in the energy propagation. However, in some of our experiments, wave envelopes do have a tendency to decline in the far left end (See e.g., Figs. 12b and 20b). It is conjectured that, when wave reaching this area, they were subjected to the effects of bottom floor and reflection, which all tend to diminish waves by their own ways.

As comparison, numerical analyses were also carried out using the same nondimensional periods: $\sigma^2 h/g$ = 0.3 and 0.5, with same slopes variations: s = 0, 2, and 4, together with the depth relations: q = 0.1, 0.2. The results are presented in Figs. 10a to 21a, in time intervals of T/8. In these figures, surface elevations resulted from solutions of finite amplitude waves.

As can be seen, the agreements of the characteristics of surface variations between these results are rather satisfactory.

## 6 CONCLUSIONS

Boundary element method has been applied to study deformations of finite amplitude waves passing variable sea floor topography. Numerical results were compared with experiments, the results are in satisfactory agreements. It is thus concluded that, for studying wave transformations due to sea floor topography, boundary element method is an efficient method to apply.

## 7 REFERENCES


Chou, C.R. 1983 "Application of Boundary element method on water wave problems" Rep. Dept. River & Harbor Engng. National Taiwan Ocean Univ. Keelung, Taiwan (in Chinese)

Chou, C.R. & C.Y. Yueh & W.K. Weng 1989 "Numerical solution for nonlinear wave" 10th Conf. Ocean Engng. Taipei, Rep. China October, pp 617 - 627 (in Chinese)


Table 1 Number of the segments used for the cases studied

| S | $N_1$ | $N_2$ | $N_3$ | $N_4$ | Total |
|---|---|---|---|---|---|
| 0 | 10 | 100 | 10 | 120 | 240 |
| 5 | 10 | 125 | 10 | 125 | 270 |
| 10 | 10 | 150 | 10 | 150 | 320 |
| 20 | 10 | 200 | 10 | 200 | 420 |

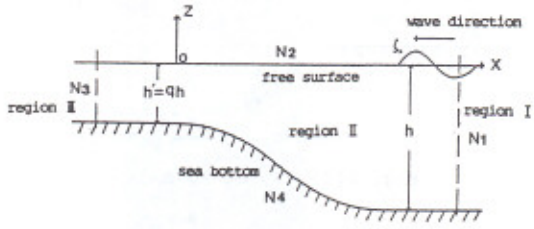


(a) origin within sub-region II

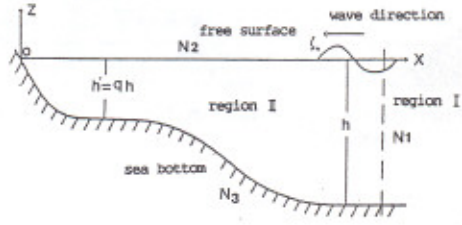


(b) origin on sub-region II

Fig.1 Definition sketches for the cases studied.

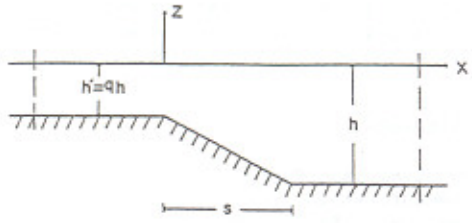


Fig. 2(a) Gradually varying sea bottom

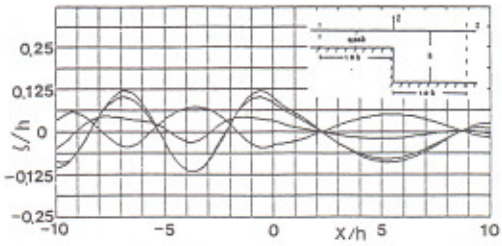


(a) S = 0

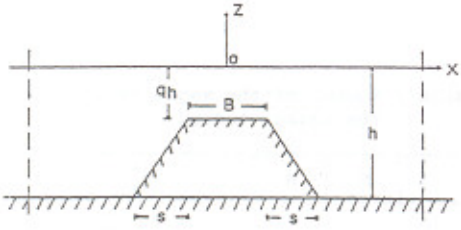


Fig. 2(b) Submerged trapezoidal dike

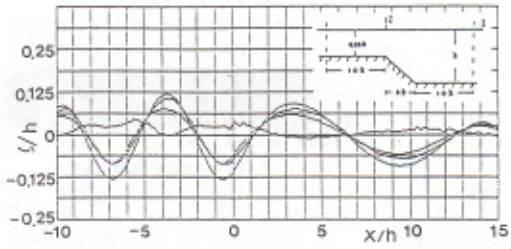


(b) s = 5h

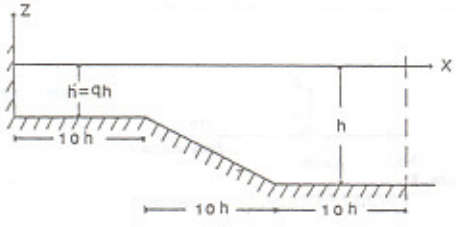


Fig. 2(c) The steep-bank

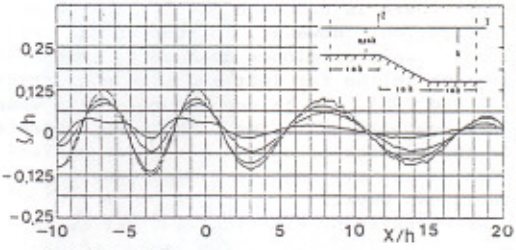


(c) S = 10h

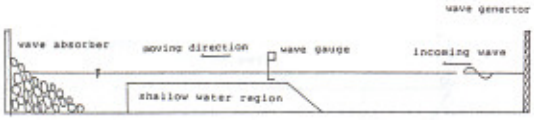


Fig.3 Schematic diagram for the experimental setups

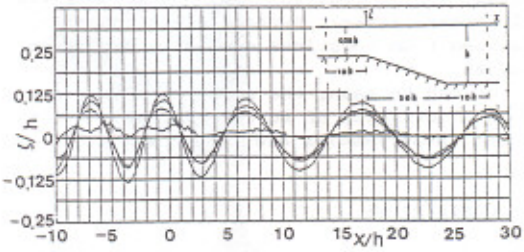


(d) S = 20h

Fig.4 Water surface undulations for various bed lopes. Water depth qh = 0.25h, incident waves with dimensionless frequency $\sigma^2 h/g = 0.25$; dimensionless amplitude $\zeta_a/h = 0.05$:

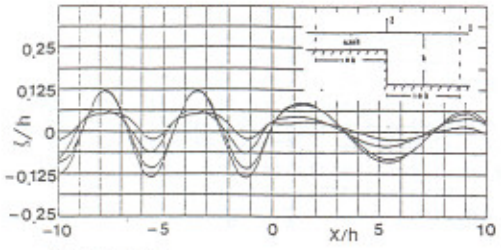


(a) S = 0

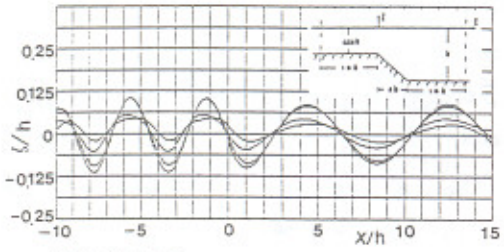


(b) S = 5h

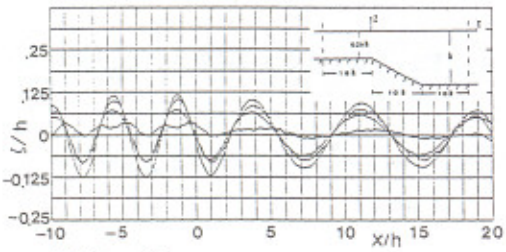


(c) S = 10h

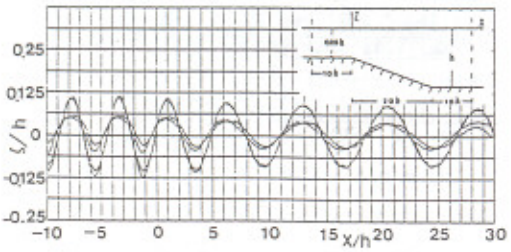


(d) S = 20h

Fig.5 Water surface undulations for various bed lopes. Water depth qh = 0.25h, incident waves with dimensionless frequency $\sigma^2 h/g$ = 0.5; dimensionless amplitude $\zeta_a/h$ = 0.05:

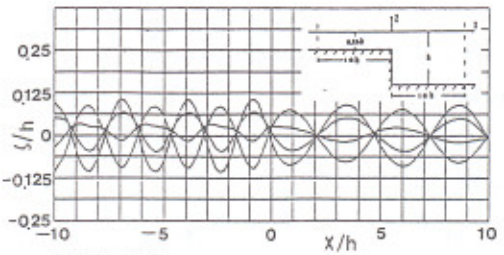


(a) S = 0

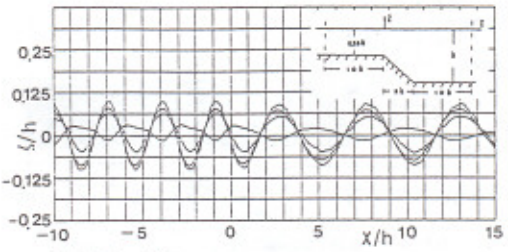


(b) S = 5 h

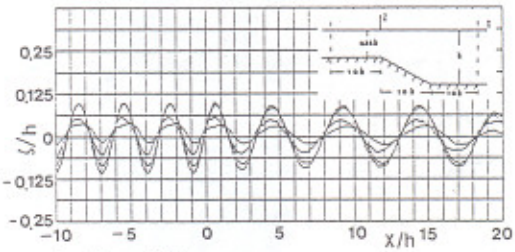


(c) S = 10h

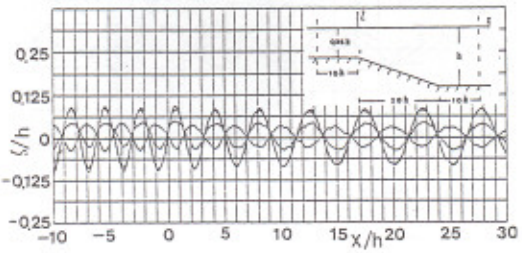


(d) S = 20h

Fig.6 Water surface undulations for various bed lopes. Water depth qh = 0.25h, incident waves with dimensionless frequency $\sigma^2 h/g$ = 1.0; dimensionless amplitude $\zeta_a/h$ = 0.05:

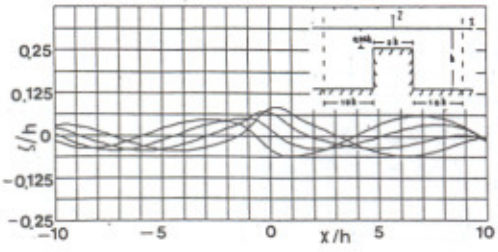


(a) $\sigma^2 h/g = 0.25$

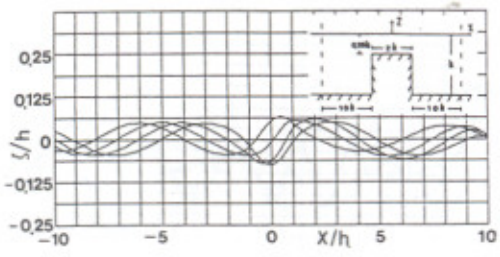


(b) $\sigma^2 h/g = 0.50$

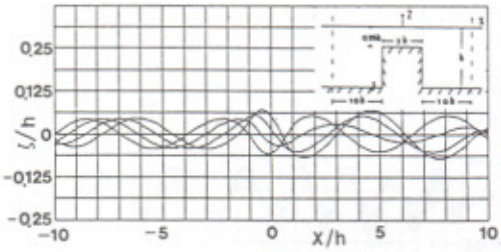


(c) $\sigma^2 h/g = 0.75$

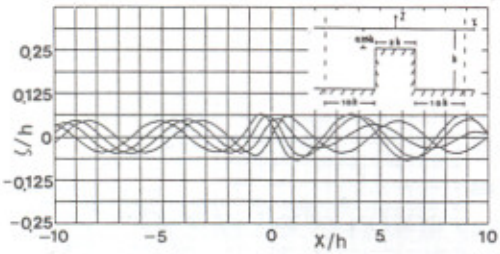


(d) $\sigma^2 h/g = 1.0$

Fig.7 Water surface undulations over a rectangular shaped dike. Depth of submergence q = 0.25

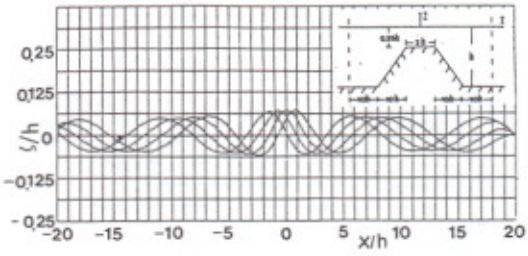


(a) $\sigma^2 h/g = 0.25$

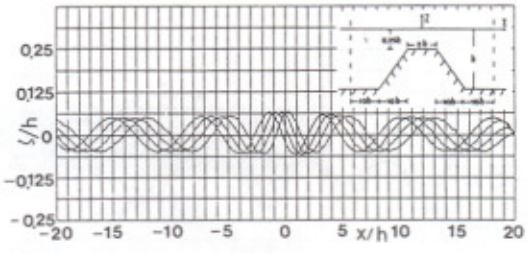


(b) $\sigma^2 h/g = 0.50$

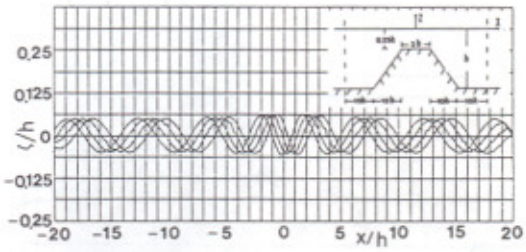


(c) $\sigma^2 h/g = 0.75$

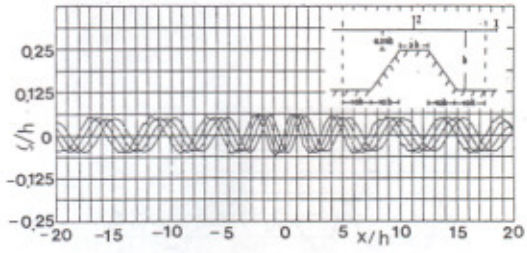


(d) $\sigma^2 h/g = 1.0$

Fig.8 Water surface undulations over a trapezoidal dike. Depth of submergence q = 0.25. Slope S = 10h.

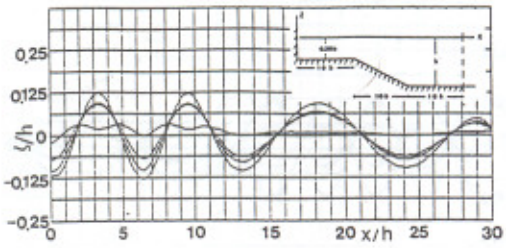


(a) $\sigma^2 h/g = 0.25$

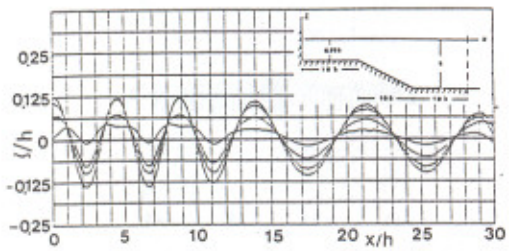


(b) $\sigma^2 h/g = 0.50$

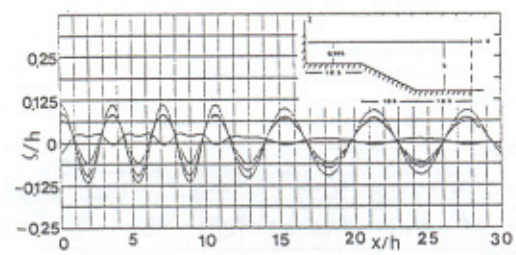


(c) $\sigma^2 h/g = 0.75$

Fig.9 Water surface undulations due to the presence of a steep bank. Depth of submergence q = 0.25. Slope S = 10h.

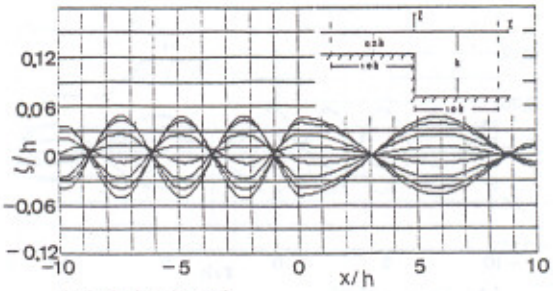


(a) Calculated

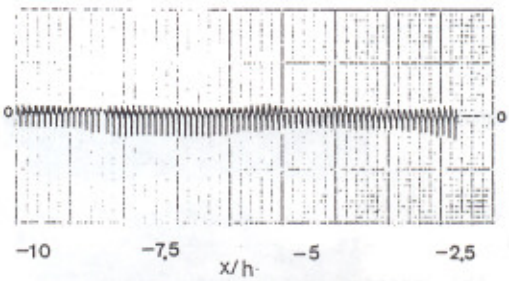


(b) recorded surface undulations

Fig.10 Calculated water surface elevations in comparison with the experimental results for the case of a steep bank. $\sigma^2 h/g = 0.3$; S = 0; and q = 0.2.

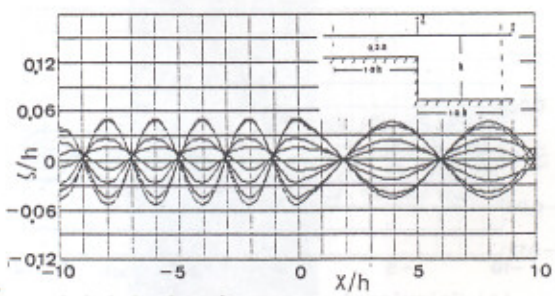


(a) Calculated

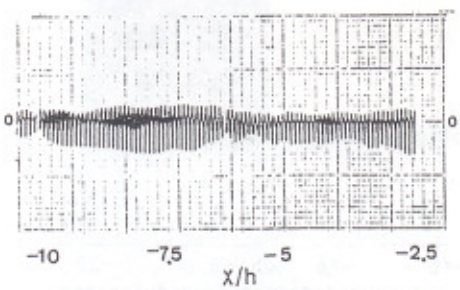


(b) recorded surface undulations

Fig.11 Calculated water surface elevations in comparison with the experimental results for the case of a steep bank $\sigma^2 h/g = 0.5$; s = 0; and q = 0.2

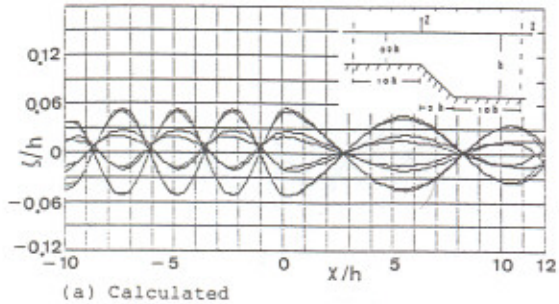


(a) Calculated

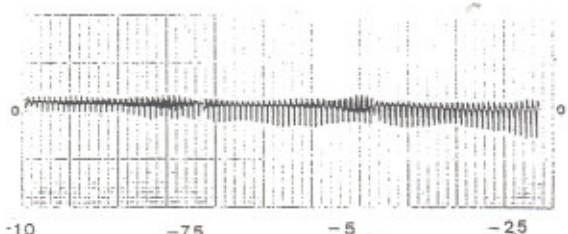


(b) recorded surface undulations

Fig.12 Calculated water surface elevations in comparison with the experimental results for the case of sloping beach $\sigma^2 h/g = 0.3$; $s = 2h$; and $q = 0.2$

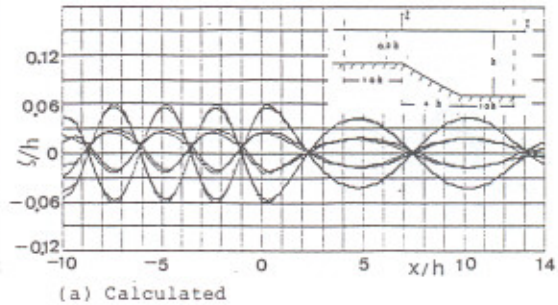


(a) Calculated

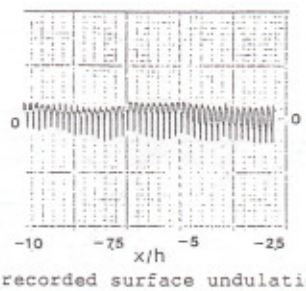


(b) recorded surface undulations

Fig.14 Calculated water surface elevations in comparison with the experimental results for the case of sloping beach. $r^2 h/g = 0.3$; $s = 4h$; and $q = 0.2$.

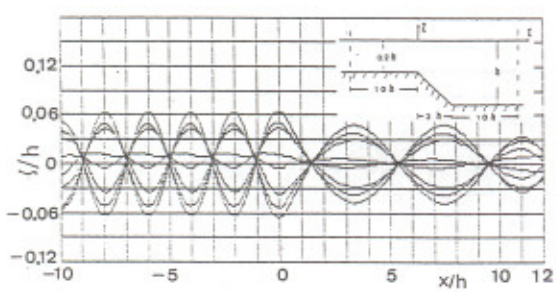


(a) Calculated

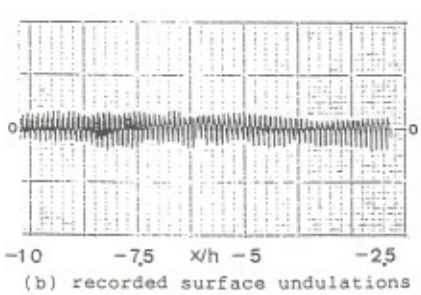


(b) recorded surface undulations

Fig.13 Calculated water surface elevations in comparison with the experimental results for the case of sloping beach $\sigma^2 h/g = 0.5$; $s = 2h$; and $q = 0.2$.

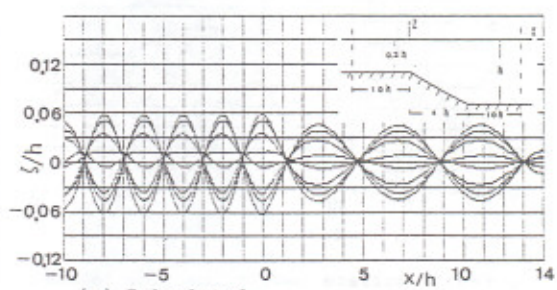


(a) Calculated

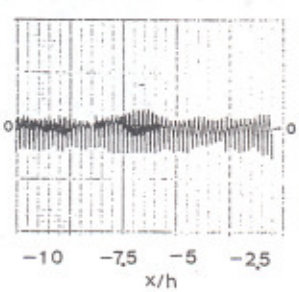


(b) recorded surface undulations.

Fig.15 Calculated water surface elevations in comparison with the experimental results for the case of sloping beach $r^2 h/g = 0.5$; $s = 4h$; and $q = 0.2$.

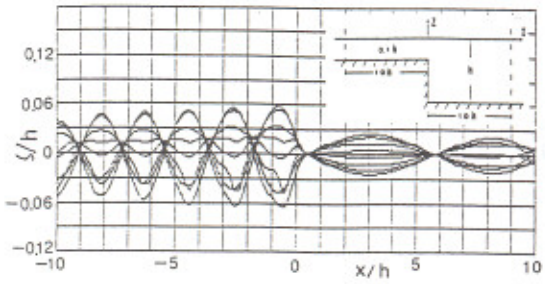


(a) Calculated

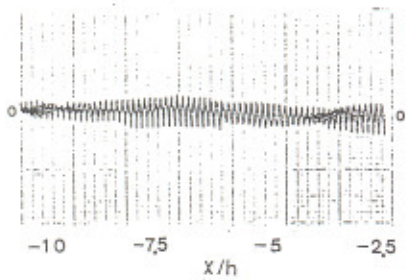


(b) recorded surface undulations

Fig.16 Water surface elevations for waves passing through a steep bank. With $\sigma^2 h/g = 0.3$; $s = 0$; and $q = 0.1$.

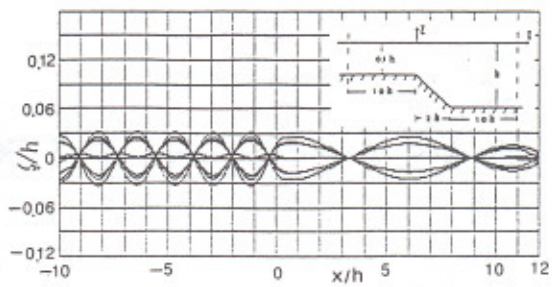


(a) Calculated

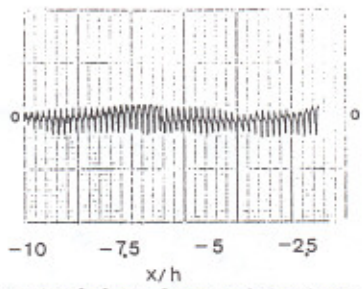


(b) recorded surface undulations

Fig.18 Water surface elevations for waves passing through a sloping beach. With $\sigma^2 h/g = 0.3$; $s = 2h$; and $q = 0.1$.

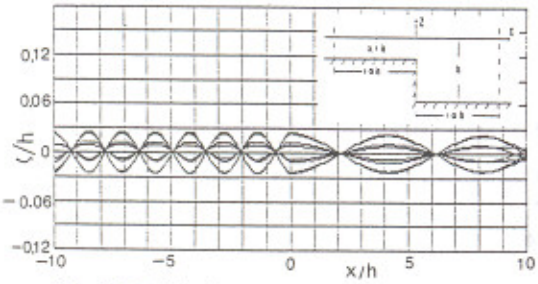


(a) Calculated

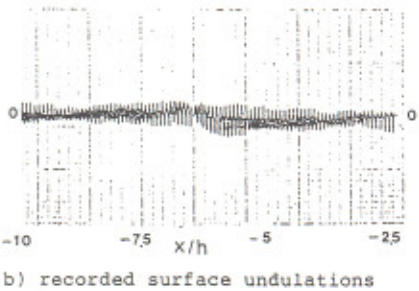


(b) recorded surface undulations

Fig.17 Water surface elevations for waves passing through a steep bank. With $\sigma^2 h/g = 0.5$; $s = 0$; and $q = 0.1$.

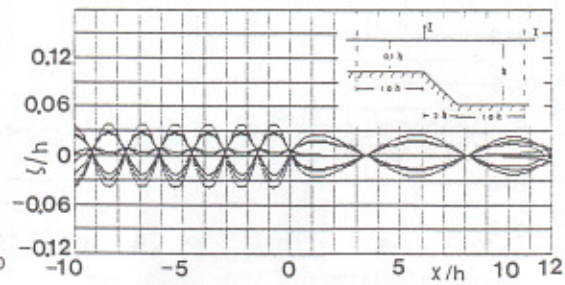


(a) Calculated

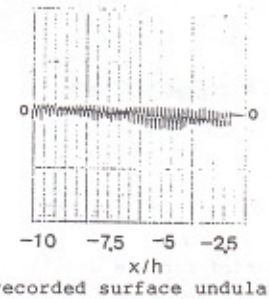


(b) recorded surface undulations

Fig.19 Water surface elevations for waves passing through a sloping beach. With $\sigma^2 h/g = 0.5$; $s = 2h$; and $q = 0.1$.

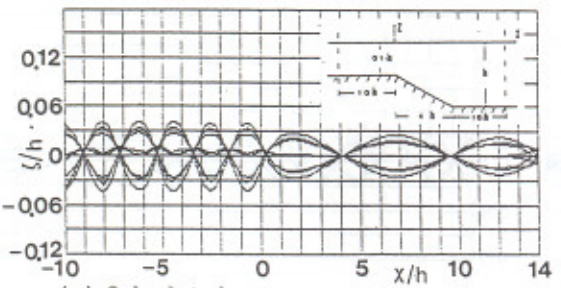


(a) Calculated

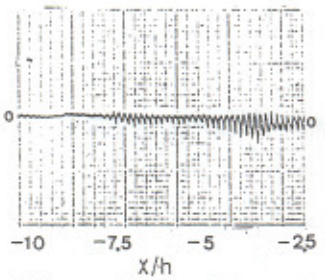


(b) recorded surface undulations

Fig.20 Water surface elevations for waves passing through a sloping beach. With $\sigma^2 h/g = 0.3$; $s = 4h$; and $q = 0.1$.

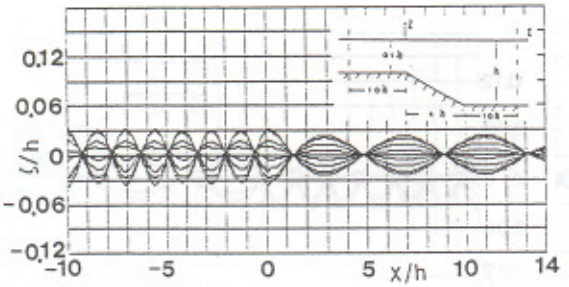


(a) Calculated

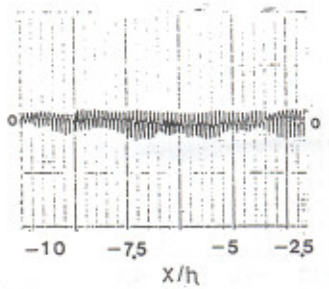


(b) recorded surface undulations

Fig.21 Water surface elevations for waves passing through a sloping beach. With $\sigma^2 h/g = 0.5$; $s = 4h$; and $q = 0.1$.